Published in Solar Energy Materials and Solar Cells 86, issue 3, 385-397, 2005
which should be used for any reference to this work

Low pressure chemical vapour deposition of ZnO layers for thin-film solar cells: temperature-induced morphological changes

S. Fay*, U. Kroll, C. Bucher, E. Vallat-Sauvain, A. Shah

Institut de Microtechnique (IMT), Thin-film Silicon and Photovoltaics Laboratory, Rue A.-L. Breguet 2, 2000 Neuchâtel, Switzerland

Abstract

Zinc oxide (ZnO) is now often used as a transparent conductive oxide for contacts in thin-film silicon solar cells. This paper presents a study of ZnO material deposited by the low-pressure chemical vapour deposition technique, in a pressure range below the pressures usually applied for the deposition of this kind of material. A temperature series has been deposited, showing a morphological transition around 150 °C. ZnO samples deposited with temperatures just higher than this transition are constituted of large grains highly oriented along a single crystallographic orientation. These "monocrystals" lead to low resistivity values, showing a clear correlation between the size of the surface grains and the electrical performance of corresponding films. Additionally, these large grains also yield ZnO layers with high transparency and high light-scattering power, specially suitable for solar cell technology based on thin-film silicon.

Keywords: Tco; Lp-cvd; Zinc oxide; Growth; Thin-film solar cells

*Corresponding author.
E-mail address: sylvie.fay@unine.ch (S. Fay).¨

1. Introduction

Transparent conductive oxides (TCO) have optical and electrical properties that make them well suited to act as transparent contacts for thin-film solar cell technology. Amongst these, zinc oxide (ZnO) is at present more and more used as TCO for thin-film solar cells, because of its low cost and the wide availability of its constituent raw materials. Intrinsic ZnO is a transparent material that can be rendered conductive either through an excess of zinc, or through vacancies of oxygen, in the ZnO lattice; both effects result in an n-type conductivity. However, this "intrinsic" conductivity of ZnO is not high enough as to enable ZnO layers to act as an electrical contact for thin-film solar cells. Therefore, ZnO layers are doped to enhance further their n-type conductivity, using dopants such as aluminium, boron, fluor, gallium, indium, etc. [1].

The basic properties of ZnO layers used as contact layers in thin-film silicon solar cells are, thus, a high value of optical transparency in the required spectral range (mainly in the visible spectral range but also in the near-infrared (NIR)), as well as a sufficiently high value of electrical conductivity. A further property of TCO layers used in thin-film solar cells is their capacity to scatter the incoming light, particularly the long wavelength light (red and NIR). This scattering effect enhances the path of the light inside the solar cell, and therefore also enhances its probability to be absorbed by the cell. This property is especially important in the case of amorphous and microcrystalline silicon (a-Si:H and μc-Si:H) thin-film solar cells, because of their relatively low optical absorption coefficient in the red and NIR spectral range. Moreover, thicker a-Si:H ($>0.4\,\mu m$) and μc-Si:H ($>3\,\mu m$) intrinsic(i)-layers cannot be used within the corresponding solar cells, because (a) the light-induced degradation effect (Staebler–Wronski effect) in a-Si:H p–i–n solar cells becomes more pronounced as the thickness of the a-Si:H i-layer is increased, and because (b) the deposition times needed for thicker silicon layers become so long that cell manufacturing becomes economically prohibitive (especially in the case of μc-Si:H solar cells). The light scattering property is linked to the surface roughness of the TCO layer used in the cell. Indeed, a rough surface allows one to scatter efficiently the light that enters into the solar cells through the TCO layer.

Up to now, sputtered ZnO has been widely used in R&D work on thin-film solar cells. Sputtering technique yields flat ZnO layers; they can be subsequently roughened (textured) through a post-etching process [2,3]. Incorporation of such sputtered and post-etched layers in entire a-Si:H and μc-Si:H solar cells has yielded excellent results [4]. However, the post-etching step could turn out to be a critical step when upscaling the manufacturing process for actual commercial module production (because of production hazards and material waste). It would therefore be desirable to have a deposition process that yields as-grown rough ZnO layers. This can be obtained, under certain conditions, with the chemical vapour deposition (CVD) process. Three different forms of CVD have been so far studied for deposition of ZnO layers for the use in solar cells and other optoelectronics devices: atmospheric pressure CVD (AP-CVD), low pressure CVD (LP-CVD), and plasma enhanced CVD (PE-CVD). The latter, as used for doped ZnO deposition, is in a very

early stage of preliminary investigations [5,6] and will not be further treated in the present paper. A comprehensive study of ZnO deposited by AP-CVD using different dopants has been conducted by Hu and Gordon [7–10]. Much of the research work that has been done on doped or undoped ZnO deposited by AP-CVD show a clear dependency of the optical, electrical and structural properties of the ZnO on the deposition temperature. However, the typical deposition temperature for the AP-CVD technique is around 400 °C, which remains quite high for thin-film solar cell technology. Lowering the pressure allows one to reduce the deposition temperature.

The present paper will, therefore, be focused on LP-CVD deposition of ZnO. Indeed, with the goal of improving the control of the chemical reactions involved in the deposition process, of improving the thickness homogeneity of the resulting layers, and of possibly reducing the deposition temperature, several researchers have investigated LP-CVD processes for ZnO (see e.g. [11]). Patents have been deposited on the LP-CVD process for doped ZnO [12,13]. Addonizio et al. [14] obtained LP-CVD ZnO layers with optimized morphological and electrical properties in the process pressure range of 1–4 Torr. They observed also a strong variation of the surface morphology as a function of the deposition temperature. Wenas et al. [15] have varied the process pressure between 12 and 20 Torr. They observed that premature reactions can occur in the vapour phase as the total process pressure is increased. This confirms the fact that a better control of the growth of ZnO can be achieved by reducing the process pressure. Wenas et al. also observed a morphological transition while increasing the deposition temperature for ZnO deposited at 6 Torr [16]. Furthermore, they highlighted the necessity to further improve the grain structure of ZnO films, in order to enhance the electrical properties of ZnO layers.

In the present study, ZnO layers have been deposited by LP-CVD, in a pressure range inferior to 1 Torr, well below the ones reported in the studies mentioned above; our goal has thereby been to incorporate such layers as front TCO layers in microcrystalline/amorphous or ''micromorph'' tandem thin-film silicon solar cells (see [17] for a detailed description of such ''micromorph'' solar cells). Under our deposition conditions, a ZnO with a marked preferential crystallographic growth and surface roughness, well suited for light scattering in thin-film solar cells has been obtained.

2. Experimental

ZnO layers have been deposited by LP-CVD. Diethylzinc (DEZ) and water (H_2O) vapours have been used as precursors, and directly evaporated in the system. In this case, the vapours were not diluted in a carrier gas. Diborane (B_2H_6) has been used as doping gas, 2% diluted in Helium. DEZ and H_2O flows have been set to 13.5 and 16.5 sccm, respectively. The total pressure was kept at 0.5 mbar (~0.37 Torr). As the deposition temperature has been clearly identified to be the predominant parameter controlling most of the electro-optical properties of the ZnO films, a temperature

series has been deposited, tuning the temperature from 130 to 235 °C. The thickness of the ZnO samples has been kept between 2 and 2.5 μm.

Thickness has been measured using a profilometer, and the deposition rate has been deduced from this measurement. Resistivity has been measured by the four-probe method [18]. Optical transmittance, both total and diffuse, have been measured using a spectrometer with an integrating sphere, in the visible and NIR wavelength range. X-ray diffraction (XRD) measurements and transmission electron microscopy (TEM) cross-sections have been performed to characterize the crystallographic orientation and the microstructure of the ZnO layers. Finally, surface topography images have been taken by scanning electron microscopy (SEM) to analyse the surface morphology of the ZnO samples.

3. Results and discussion

The present study was conducted, in a first instance, on undoped ZnO layers. In fact, for a practical use within thin-film solar cells, it will generally be necessary to keep the doping level relatively low in order to minimise the free carrier absorption in the NIR, while still maintaining a sufficient electrical conductivity. Indeed, the free carrier absorption is proportional to the density N_e of free electrons in the ZnO layers, and is increased if the doping level is augmented. On the other hand, the electrical conductivity σ is given by the relationship $\sigma = qN_e\mu_e$, where q is the elementary charge and μ_e is the electron mobility, so that a minimum N_e is necessary to get acceptable conductivity values, even if the latter can be further enhanced by improving the electron mobility.

By investigating at first undoped ZnO layers we are able to get a general picture on how process parameters influence layer properties. Subsequently, we have introduced, for the so far optimized process conditions, doping by Boron so as to obtain the necessary higher conductivity at a relatively low dopant concentration.

3.1. Undoped ZnO layers

The deposition rate, as shown in Fig. 1, increases with the temperature. As in the low-pressure regime, the CVD process is more kinetic limited than diffusion limited, the observed increase of the deposition rate is probably due to the increase of the kinetic reaction process at the growth surface. Indeed, at higher temperatures more thermal energy is available, and therefore the chemical reactions which take place at the growth surface are accelerated. Therefore, high temperature is basically beneficial with respect to the deposition rate.

Surprisingly, the growth of the ZnO films follows another trend which is not linked to the deposition rate behaviour, and is shown in Fig. 2: indeed, the XRD patterns show a clear change of the growth direction, from a preferential orientation along the (0002) crystallographic plans to a preferential orientation along the $(1\,1\,\bar{2}\,0)$ crystallographic plans as the deposition temperature is increased. This abrupt transition in the crystallographic preferential growth direction is accompanied with a

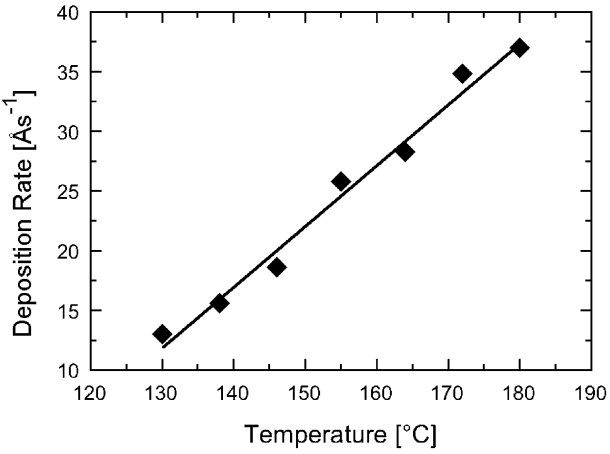

Fig. 1. Deposition rate of undoped ZnO layers as a function of the substrate temperature, for a total pressure of 0.5 mbar.

morphological change of the growing surface, as observed in the SEM micrographs of the ZnO films surface (see Fig. 2). Above 145 °C, large tetragonal grains having their growth axis preferentially oriented perpendicular to the $(1\,1\,\bar{2}\,0)$ crystallographic plans emerge out of the surface. If the temperature is further increased, the size of these large grains decreases, and at even higher temperatures ($T = 235$ °C), the growth of the ZnO layers becomes disordered, with the apparition in the XRD of multiple growth orientations. Such a morphological transition depending on temperature has also been reported in previous papers, for higher deposition pressures. However, in our case the surface morphology just after the transition is definitively different, with larger tetragonal grains; furthermore, instead of having two XRD peaks ($(1\,1\,\bar{2}\,0)$ and $(1\,0\,\bar{1}\,0)$) for the ZnO layers deposited after the transition (as one observes at higher pressure [16]), only a single XRD peak pertaining to the $(1\,1\,\bar{2}\,0)$ crystallographic plans appears significantly here. This suggests that the ZnO films deposited at lower pressures (<1 mbar) are more oriented along a single preferential orientation. Fig. 3 shows a SEM micrograph of the surface of a ZnO layer deposited at 155 °C, i.e. just after the morphological transition. The measured size of the tetragonal basis of the grains emerging out of the surface is ~400 nm. On the other hand, grain size δ calculated with the Sherrer equation from the full-width at half-maximum (FWHM) value of the XRD spectra yields values of $\delta \sim 30$ nm. This discrepancy can be understood by looking at the cross-sectional TEM micrograph given in Fig. 4. The microstructure of the films consists of small crystallites at the bottom of the films, followed by the growth of larger crystals that emerge with crystallographically well-defined facets at the surface (it has to be noted, however, that the topography of the crystals emerging at the sample surface in this Fig. 4 is not representative, because of the ion-milling thinning

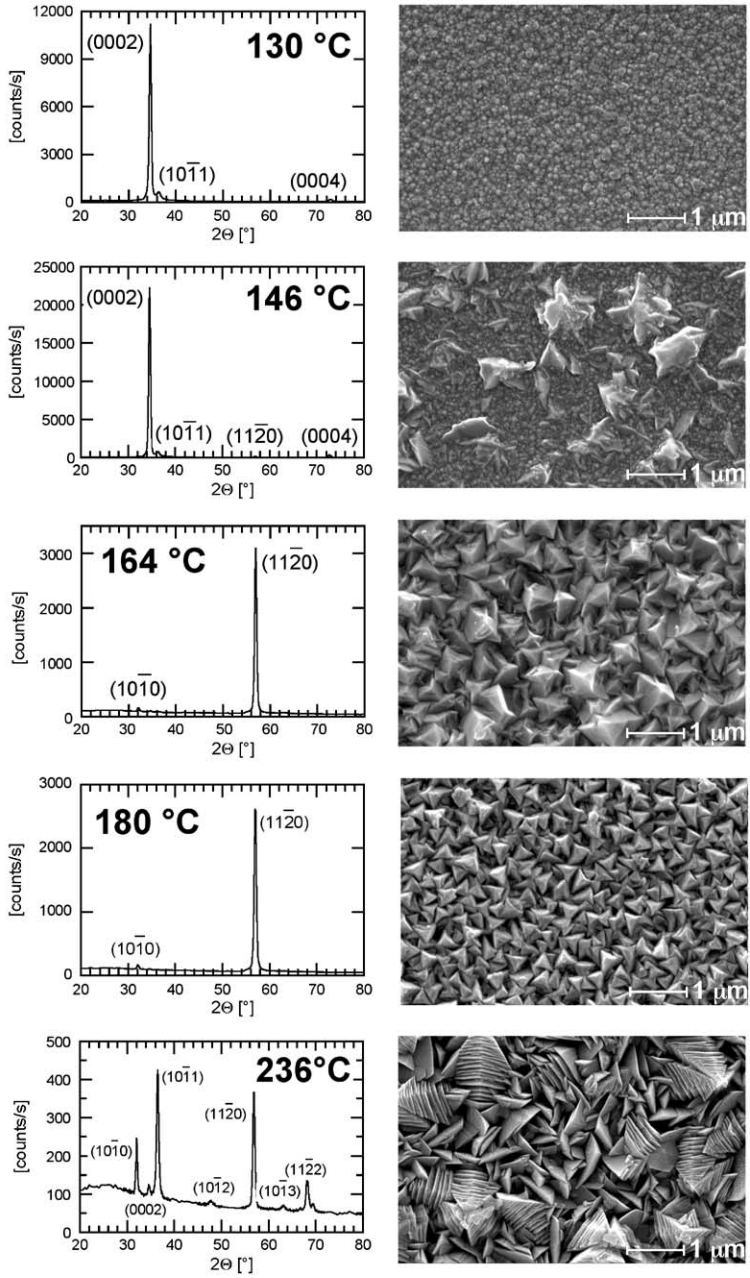

Fig. 2. SEM micrographs and corresponding XRD spectra of undoped ZnO layers as a function of the substrate temperature, for a total pressure of 0.5 mbar.

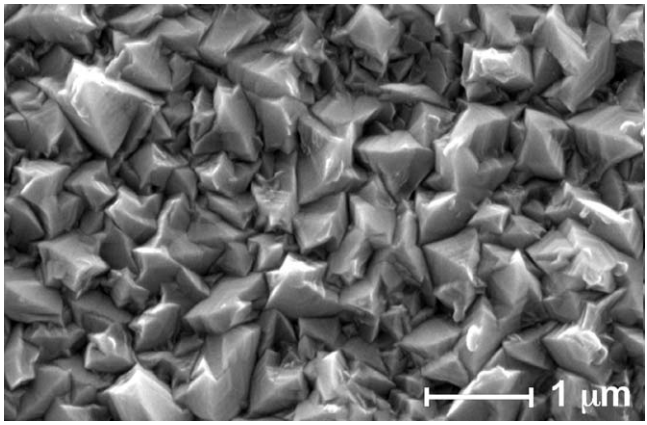

Fig. 3. SEM micrograph of an undoped ZnO layer deposited at 155 °C, at a pressure of 0.5 mbar.

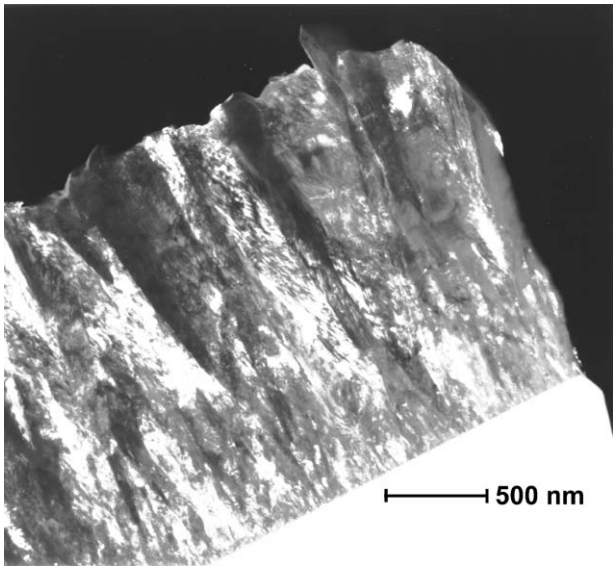

Fig. 4. TEM dark field micrograph of an undoped ZnO layer deposited at 164 °C. In the first 200 nm, the microstructure consists of small randomly oriented crystallites, whereas for a thickness larger than 500 nm, one can observe large conical crystals. Note that the topography of the crystals emerging at the sample surface is not representative because of the ion-milling thinning of the TEM samples that eroded the characteristic tetrahedrons, as seen in Fig. 3.

of the TEM samples that eroded the characteristic tetrahedrons, as seen on Fig. 3). As crystals of dimensions larger than 0.5 μm do not contribute to a significant broadening of the XRD peak, we can safely assume that the smallest crystals at the bottom of the layer are responsible for the observed broadening of the XRD peak.

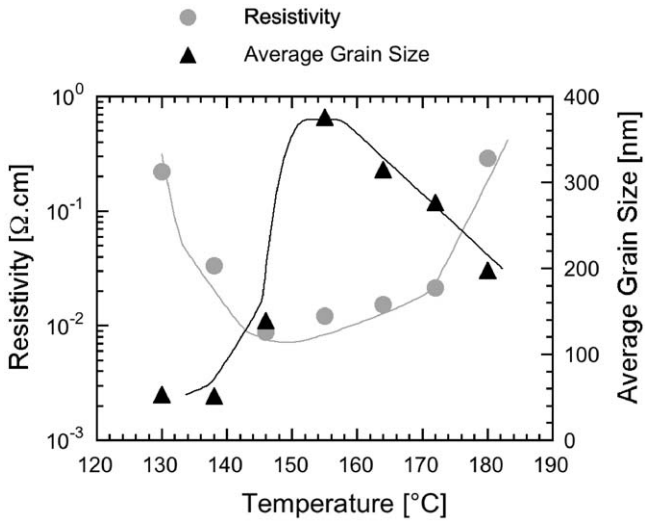

Fig. 5. Resistivity of undoped ZnO layers and average size of the grains emerging out of the ZnO layers surface, as a function of the substrate temperature.

In Fig. 5, the variation of resistivity as a function of substrate temperature is shown: the resistivity drops almost 2 orders of magnitude around 150 °C, i.e. at the morphological transition mentioned previously, and increases again after 170 °C. The lowest value of intrinsic resistivity is obtained just after the morphological transition, i.e. in the range of temperatures where ZnO layers with $(1\,1\,\bar{2}\,0)$ preferential growth and large monocrystals emerging at the surface are obtained. Furthermore, for higher temperatures (235 °C) for which the deposited ZnO layers are no longer oriented along a single preferential direction, the resistivity values become very high.

Quantitative image analysis of the SEM micrographs given in Fig. 2 yields the average size of the emerging crystals as given in Fig. 5 as a function of the deposition temperature, and shown there along with the resistivity values. The average size of the emerging crystals goes through a maximum while the temperature increases. Above the temperature of the morphological transition, i.e. for crystals oriented along the $(1\,1\,\bar{2}\,0)$ crystallographic plans, the surface crystallite size decreases with increasing temperature, followed by an increasing layer resistivity. Such a behaviour can be expected if one postulates that the electron mobility decreases when the grain boundary density within the layers increases.

These observations highlight the importance to have an improved ZnO structure, i.e. at least large crystals. However, as the preferential orientation varies, as does the crystal size, it is not clear whether both conditions (large grain size and strong preferential orientation) are needed to achieve high conductivities.

Optical total and diffuse transmittance spectra of the temperature series of undoped ZnO, deposited at 0.5 mbar, are shown in Fig. 6. The total transmittance does not vary strongly with the substrate temperature, and there is no drop of the total transmittance in the NIR wavelength range. The latter can be explained by the

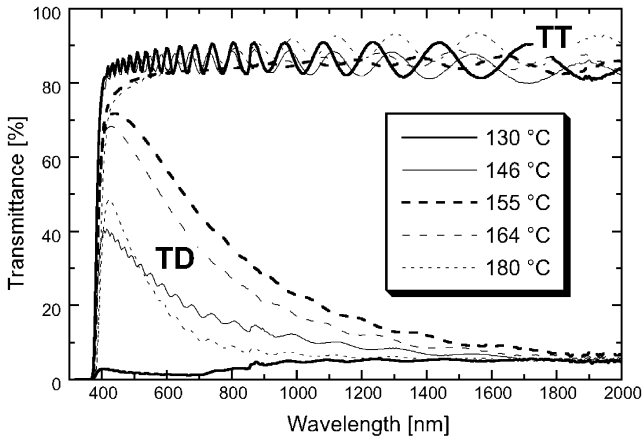

Fig. 6. Total and diffuse transmittance of temperature series of undoped ZnO layers deposited at 0.5 mbar.

fact that the ZnO samples of this series are undoped and the density of free carriers in the films is here, thus, not high enough to lead to substantial free carrier absorption in this wavelength range.

On the other hand, the diffuse transmittance does vary considerably with substrate temperature (even though all the films have the same thickness). It increases until the transition is achieved (i.e. $\sim$155 °C), and decreases again for higher temperatures, following a similar trend (but inverted) as the one observed for the resistivity. This means that the optimum conditions for light scattering are obtained at the same temperature, for which the optimum for the resistivity is obtained, i.e. just after the morphological transition. Comparing this trend for the diffuse optical transmittance with the SEM micrographs of Fig. 2, it becomes evident that the large grains obtained just after the transition at 155 °C are responsible for the high value of the diffuse optical transmittance spectrum, as measured at 155 °C. For higher substrate temperatures, the size of the grains decreases again, as does the diffuse optical transmittance of the ZnO layers.

ZnO samples deposited at this optimal temperature of around 155 °C have a good optical transparency (for the wavelength range from 350 nm right up to the NIR area), a resistivity with a minimum value of $1.10^{-2}\,\Omega$cm obtained, thanks to the presence of large grains with a pronounced crystallographic orientation, and a high capacity to scatter light. However, the resistivity obtained in this series is still too high, so that one cannot use these undoped ZnO directly as electrical contact layers for our thin-film silicon solar cells, and doping is indeed to be performed.

3.2. Doped ZnO layers

In order to observe the effect of incorporation of Boron into the ZnO layers, a doping series has been deposited at 155 °C and 0.5 mbar, thereby steadily increasing the B_2H_6/DEZ ratio.

The effect of doping on the resistivity of the ZnO layers is illustrated in Fig. 7. The introduction of active dopants with the corresponding increase in free carrier density leads to a strong drop in the resistivity. Thus, by adding Boron as dopant into the ZnO layers, the resistivity can be lowered by one order of magnitude, achieving values around $1.10^{-3}\,\Omega\,\mathrm{cm}$, allowing such ZnO layers to be conductive enough to act as TCO contact layers for thin-film solar cell applications. However, one can also observe that, above a certain doping level ($B_2H_6/DEZ > 0.6$), a further increase of the doping does not yield a further decrease of the resistivity.

The drop of total transmittance in the NIR wavelength range due to free carrier absorption is shown in Fig. 8. This drop should in principle be as low as possible, because it occurs in a wavelength range for which our "micromorph" solar cells are photovoltaically active (i.e. for photon energies above the energy gap of μc-Si:H, which is 1.12 eV). This confirms the importance of minimizing the amount of dopant needed in the ZnO film and optimizing the mobility to lower the resistivity.

In Fig. 9, we plot the $(1\,1\,\bar{2}\,0)/(1\,0\,\bar{1}\,0)$ peak ratio as a function of the B_2H_6/DEZ ratio. This $(1\,1\,\bar{2}\,0)/(1\,0\,\bar{1}\,0)$) peak ratio is very low for undoped ZnO layers deposited at 155 °C, and it remains low while the concentration of dopant is increased. Furthermore, no diffraction peak other than the $(1\,1\,\bar{2}\,0)$ peak appears significantly in the XRD spectra of our doped ZnO. The preferential growth orientation of ZnO deposited at 155 °C and at low pressure of 0.5 mbar is, therefore, not influenced by doping, and the ZnO films are still composed of strongly oriented monocrystals, even for high doping levels. It has to be noted that such a constancy of structural behaviour with a pronounced preferential growth direction, while increasing the doping level, is not observed in ZnO layers deposited at higher pressure [16]. In the latter case, the $(1\,1\,\bar{2}\,0)$ peak is predominant only for low doping levels, and the $(1\,0\,\bar{1}\,0)$ peak becomes more and more pronounced as the doping level is increased.

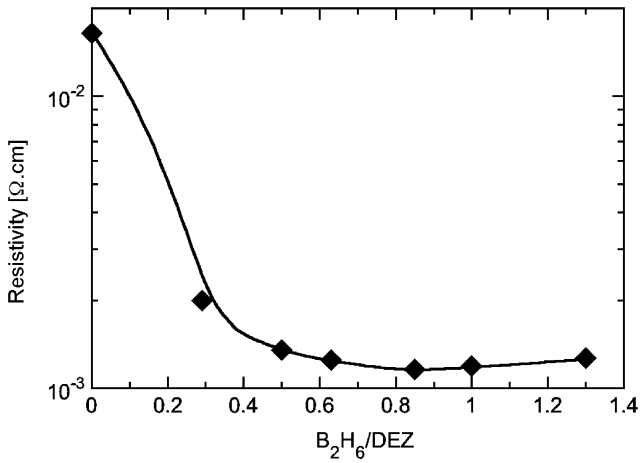

Fig. 7. Resistivity of the ZnO layers deposited at 155 °C and 0.5 mbar, as a function of the amount of dopant introduced in the chamber.

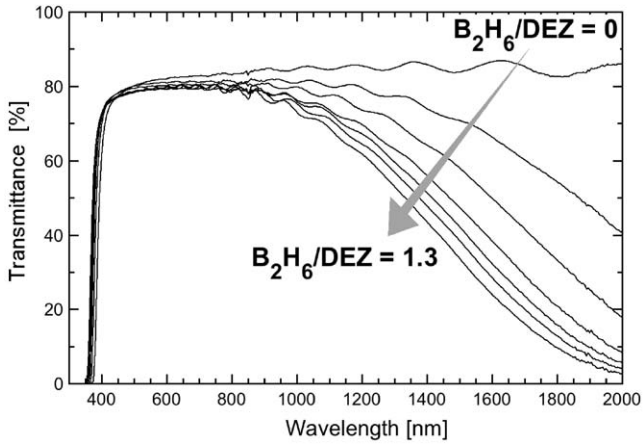

Fig. 8. Total transmittance of ZnO layers deposited at 155 °C and 0.5 mbar, as a function of the amount of dopant introduced in the chamber.

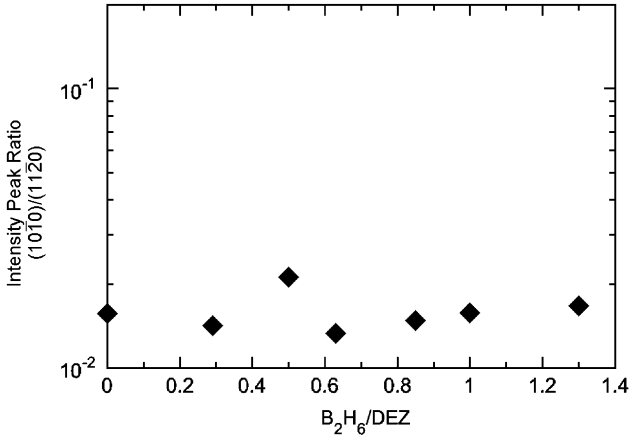

Fig. 9. Ratio of the $(1\,1\,\bar{2}\,0)$ and $(1\,0\,\bar{1}\,0)$ diffraction peaks, for ZnO layers deposited at 155 °C and 0.5 mbar, as a function of the amount of dopant introduced in the chamber. The $(1\,1\,\bar{2}\,0)$ peak is still predominant, even for high doping levels.

4. Conclusion

A temperature series of undoped ZnO has been deposited by LP-CVD at a very low pressure of 0.5 mbar. A morphological transition has been observed around 150 °C. The films deposited just after this transition exhibit a marked preferential growth orientation along the $(1\,1\,\bar{2}\,0)$ crystallographic plans and are composed of large monocrystals emerging at the surface with well-defined facets. These

monocrystals lead to low resistivity values, showing for undoped films a clear correlation between the size of the surface grains, their orientation in the ZnO film, and the electrical performances of those undoped films. Additionally, these large grains also give high values of the diffuse optical transmittance, achieving, thus, ZnO layers with high transparency and high light-scattering power.

Compared to other studies conducted at higher process pressures, the grain structure of the ZnO layers has been improved, allowing one to optimize further the electrical and optical properties of the ZnO material.

The introduction of Boron as dopant into the ZnO films did not show any influence on the growth of the ZnO layers, the latter remaining oriented along the $(1\,1\,\bar{2}\,0)$ crystallographic plans. Thereby, good electrical conductivities one order of magnitude below those of the undoped ZnO layers have been obtained.

Finally, these optimized Boron-doped ZnO layers obtained just after the transition, at 155 °C, have been successfully incorporated as front contacts into "micromorph" solar cells. Indeed, obtained stabilized cell efficiencies of over 11% show the high potential of the developed LP-CVD ZnO [19].

The morphological transition of the ZnO layers described here is observed for a wide range of process pressure, but the structure of these ZnO layers after the transition is quite different for the different pressure regimes. In our case, the decrease of the process pressure from ~6 Torr to less than 1 Torr seems to have a beneficial impact on the ZnO structure, leading to larger grains with pronounced orientation and such a structure yields good optical and electrical properties of the ZnO layers. Further investigations need to be done in this direction, in order to define the limits in possibilities of varying the process pressure, and thus, to possibly achieve even better ZnO layers.

The present study highlights the importance to have an improved structure composed of grains as large and as well oriented as possible. These grains allow one not only to achieve high conductivities, but the surface roughness that is produced by them confers to the ZnO layers also a high power for scattering the light. This property is crucial for solar cell technology based on thin-film silicon and, therefore, it is important to continue to improve the structure of ZnO layers. In this context, the CVD process seems indeed to be a very suitable process. Moreover, LP-CVD process allows one not only to decrease the deposition temperature, but also to control the process reactions in a better way and obtain thereby ZnO layers with good structural properties. Other processes using the CVD technique combined with an external, physical energy source, like PE-CVD or photo-CVD, could allow one to further improve the layer structure, allowing one to possibly approach more closely the ideal compromise between good electrical, optical, and light-scattering properties.

Acknowledgements

This work was supported by the Swiss Federal Office of Energy (OFEN) under contract No. 36487.

References

[1] R.G. Gordon, MRS Bulletin (2000) 52–57.
[2] J.A.A. Selvan, Ph.D. Thesis, Université de Neuchâtel, 1998, ISBN 3-930803-60-7.
[3] O. Kluth, A. Löffl, S. Wieder, C. Beneking, W. Appenzeller, L. Houben, B. Rech, H. Wagner, S. Hoffmann, R. Waser, J.A.A. Selvan, H. Keppner, Proceedings of the 26th IEEE Photovoltaic Specialists Conference, Anaheim, CA, 1997, 715–718.
[4] B. Rech, S. Wieder, C. Beneking, A. Löffl, O. Kluth, W. Reetz, H. Wagner, Proceedings of the 26th IEEE Photovoltaic Specialists Conference, Anaheim, CA, 1997, 619–622.
[5] K. Haga, M. Kamidaira, Y. Kashiwaba, T. Sekiguchi, H. Watanabe, J. Crystal Growth 214–215 (2000) 77–80.
[6] R. Groenen, M.C.M. van de Sanden, J. Löffler, R.E.I. Schropp, J.L. Linden, Proceedings of the IEEE Photovoltaic Specialists Conference, 2000, 822–824.
[7] J. Hu, R.G. Gordon, Solar Cells 30 (1991) 437–450.
[8] J. Hu, R.G. Gordon, J. Electrochem. Soc. 139/7 (1992) 2014–2022.
[9] J. Hu, R.G. Gordon, J. Appl. Phys. 71/2 (1992) 880–890.
[10] J. Hu, R.G. Gordon, J. Appl. Phys. 72/11 (1992) 5381–5392.
[11] A.P. Roth, D.F. Williams, J. Appl. Phys. 52/11 (1981) 6685–6692.
[12] K.A. Blaker, B. Wong, P.S. Vijayakumar, R.D. Wieting, Atlantic Richfield CO (US), 1986, Patent No EP0204563.
[13] K. Takahashi, A. Omura, M. Konagai, A. Yamada, Y. Shinichiro, M. Yoshino, Konagai Makoto and Yoshida Kogyo KK, 1996, Patent No US5545443.
[14] M.L. Addonizio, A. Antonaia, S. Aprea, R. De Rosa, G. Nobile, A. Rubino, E. Terzini, Proceedings of the second World Conference and Exhibition on Photovoltaic Solar Energy Conversion, Vienna, Austria, 1998.
[15] W.W. Wenas, Jap. J. Appl. Phys. 30/3B (1991) L441–L443.
[16] W.W. Wenas, A. Yamada, K. Takahashi, M. Yoshino, M. Konagai, J. Appl. Phys. 70/11 (1991) 7119–7123.
[17] J. Meier, P. Torres, R. Platz, S. Dubail, U. Kroll, J.A.A. Selvan, N. Pellaton-Vaucher, C. Hof, D. Fischer, H. Keppner, A. Shah, K.-D. Ufert, P. Giannoulès, J. Köhler, Proceedings of the MRS Symposium, San Francisco, 420, 1996, 3–14.
[18] F.M. Smits, The Bell System Techn. J. 37 (1958) 711–718.
[19] J. Meier, S. Dubail, S. Golay, U. Kroll, S. Faÿ, E. Vallat-Sauvain, L. Feitknecht, J. Dubail, A. Shah, Sol. Energy Mater. and Sol. Cells 74/1-4 (2002) 457–467.